Mechanism and kinetics of nano-crystallization of the thermally stable NiNb(ZrTi)Al metallic glasses

Tomasz Czeppe

Abstract The structure and crystallization of melt spun ribbons of composition $Ni_{58}Nb_x(ZrTi)_{1-x}Al_y$, ($x = 5, 10, 20,$ and 25, $y = 3, 7$ at%) were investigated. It was found that the crystallization of the amorphous phase proceeded with different phase composition and kinetics in case of the alloys containing more than 15 at% Nb. In case of the smaller content of Nb, cubic NiTi(Zr) phase crystallized rapidly. The alloy crystallized completely. In alloys with higher Nb content, a smaller volume, up to 50% of the amorphous phase crystallized much slower. The resulting phase composition contained cubic NiTi(Zr) and orthorhombic $Ni_{6.5}Nb_{6.5}$ phases. The activation energies resulting from the Kissinger and Ozawa equations were determined.

Keywords NiNbZrTiAl metallic glasses · Crystallization · Kinetics

Introduction

Bulk metallic glasses (BMG) are new class of engineering oriented materials [1]. Different families of Ni-based Nb containing amorphous alloys like: NiNbTi, NiNbZr, NiNbTiZr, NiNbZrTiAl, NiNbTiZrCoCu, NiZrNbHfAl, and NiZrTaNb revealed high glass forming ability (GFA), high fracture strength and good corrosion resistance [2–7]. Due to the small difference between heat of mixing of the pairs of elements—Nb and Zr, Zr, and Ti, Ni-based Nb containing glassy alloys may reveal good ductility [6].

T. Czeppe (✉)
Institute of Metallurgy and Materials Sciences, Polish Academy of Sciences, Reymonta 25 St, 30-059 Krakow, Poland
e-mail: nmczeppe@imim-pan.krakow.pl

A very uncommon, composition-dependent property is high thermal stability of the amorphous phase in alloys containing Hf and Ta or Al [7, 8].

In the following article the melt spun ribbons of composition $Ni_{58}Nb_x(ZrTi)_{1-x}Al_y$, ($x = 5, 10, 20, 25$ at%, $y = 3, 7$ at%), were investigated. The alloys were studied from the point of view of the microstructure, as received and after crystallization, phase composition after primary crystallization and activation energy for crystallization in continuous heating experiment. The activation energy was determined with use of the Kissinger [9] and Ozawa [10] equations basing on the peak temperature dependence on the heating rates.

Experimental

The high purity components, at least 99.99, were used for casting the alloys, later several times re-melted with use of the levitation method and finally shaped. The ribbons 50 μm thick and 5 mm wide were prepared by melt spinning. The thermal stability and the crystallization process was studied with use of the DSC DuPont 910 and with differential thermal analyser TA Instruments SDT Q600, during continuous heating with the rates 5–70 K/min, under argon protection atmosphere. To determine the crystallizing phases and the amount of crystallization the XRD Philips PW1830 and Cu Kα radiation were used. Also, transmission electron microscopes Philips CM 200, operating at 200 kV, and TECNAI G F20 (FEI) for microstructural and high resolution characterization were applied. Thin foils for HREM were prepared by electropolishing and subsequently thinned with the ion gentle milling system (Technoorg Linda). The focused ion beam technique (FIB, dual beam type, FEI) was used for the

preparation of the foils from the cross-sections of the specimens.

Results and discussion

The composition, structure, and glass forming ability of the ribbons in "as received" state

The composition of the investigated alloys is given in Table 1. The Ni content 58 at% was near to the Ni content at the known Ni-based eutectic amorphous alloy $Ni_{59}Zr_{20}Ti_{21}$. The Nb addition was used to increase ductility of the glass [6]. The Nb content increased from 5 to 25 at%, on the cost of the lowering the Zr and Ti contents. To improve glass forming ability Al addition was used [6]. The addition was 3 at%, except for the alloy Nb-3, where it increased up to 7 at%. The investigated compositions are shown in the fragment of the composition triangle in Fig. 1.

As was confirmed with the XRD (Fig. 2) and transmission electron microscopy (TEM) the structure of all ribbons was amorphous. Some typical TEM micrographs concerning alloys Nb-3 containing 10 at% Nb and Nb-4 containing 20 at% Nb, are shown in Fig. 3a–f. The broad intensity at the XRD patterns, modulated contrasts at the bright field (BF) and dark field (DF) micrographs, also ring type diffraction patterns (SADP) from the ribbons are typical for the amorphous structure. Further high resolution (HREM) observation of the ribbons, performed after

Table 1 Nominal composition of the investigated alloys

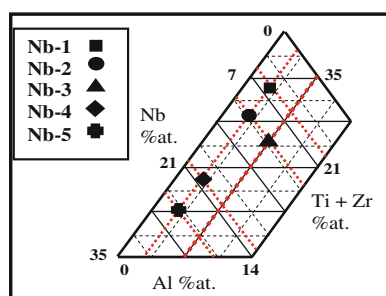|	Composition of the alloys/at%				
	Ni	Nb	Zr	Ti	Al
Nb-1	58.0	5.0	18.0	16.0	3.0
Nb-2	58.0	10.0	15.0	14.0	3.0
Nb-3	58.0	10.0	13.0	12.0	7.0
Nb-4	58.0	20.0	10.0	9.0	3.0
Nb-5	58.0	25.0	8.0	6.0	3.0

Fig. 1 Schematic presentation of the investigated compositions

additional gentle milling, also did not revealed any crystalline phase. Calorimetry and thermal analysis were used to determine the range of the thermal stability of the glasses. Glass transition temperature T_g, primary crystallization temperature T_x and temperatures of solidus and liquidus were determined for the parameters related to the glass forming ability (GFA). All the characteristic temperatures were assumed as the onset temperatures of transformations. As in the case of the investigated compositions the temperature range of crystallization exceeded 973 K, upper limit of the application of the DSC, the DTA signal registered on the SDT Q600 thermo-analyzer was used (Fig. 4). The figures demonstrate that glass transition temperature increased with the Nb content (Table 2). The GFA related parameters: reduced T_g and T_x temperatures revealed different behavior and did not supply any consistent information concerning relation between GFA and the Nb content. The ΔT parameter suggests general decrease of GFA with Nb content increase (Table 2).

The crystallization process of the amorphous phase

The crystallization process revealed pronounced differences in calorimetry (Fig. 4). The SDT traces showed one crystallization effect in the case of Nb-1 and Nb-2 compositions (Fig. 4a), the second thermal effects appeared with the increase of the Al content to 7 at%, with no change in content of Nb, for the Nb-3 composition (Fig. 4b). In case of the Nb content 20 and 25 at% Nb, in the Nb-4 and Nb-5 alloys, the crystallization proceeded in three main effects (Fig. 4c). Both the primary crystallization T_x temperatures (Table 2) and the final temperature of crystallization increase with Nb content, up to 1,063 K for the alloy Nb-4 (Fig. 4c). The application of the DSC let to determine more precisely the shape of the first crystallization effects and to estimate the enthalpy of crystallization (Fig. 9). While in the case of Nb-1 and Nb-2 alloys enthalpy was above 100 J/g for the single crystallization effect, it was much smaller, 63 J/g, for the first (doubled) effect in alloys Nb-4 and Nb-5 (Fig. 9c, d). Also increase in Al content for the alloy Nb-3 decreases ΔH of the primary crystallization to 89 J/g. Concluding above results, assuming the proportion of the crystallization enthalpy to the crystallizing volume, the increase of the Al content from 3 to 7 at%, or increase of the Nb content above 20 at%, leads to the different crystallization mechanisms as well as to much smaller crystallizing volume at the stage of primary crystallization.

In order to investigate microstructure after crystallization the XRD, TEM, and HREM were used. Preliminary the samples were prepared by heating or ageing at desired temperatures (marked by arrows in Fig. 4) in the

Fig. 2 XRD patterns of the investigated ribbons: **a** Nb-1, **b** Nb-2, **c** Nb-3, (7 at% Al), **d** Nb-4, **e** Nb-5
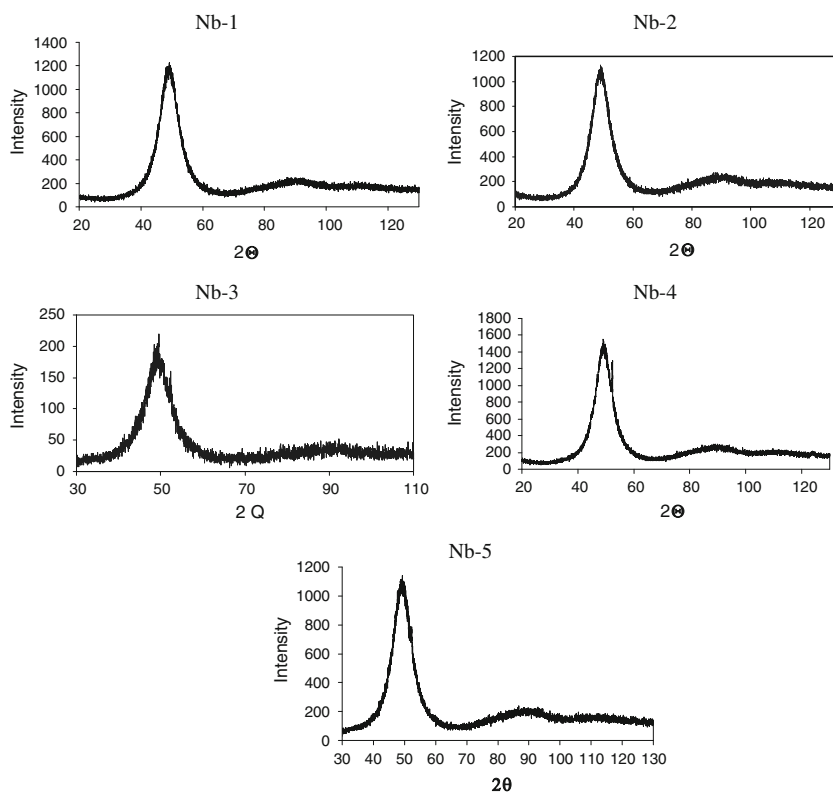

Fig. 3 The amorphous structure of the ribbons Nb-3 (**a** BF, **b** SADP, **c** DF) and Nb-4 (**d** BF, **e** SADP, **f** DF); TEM micrographs
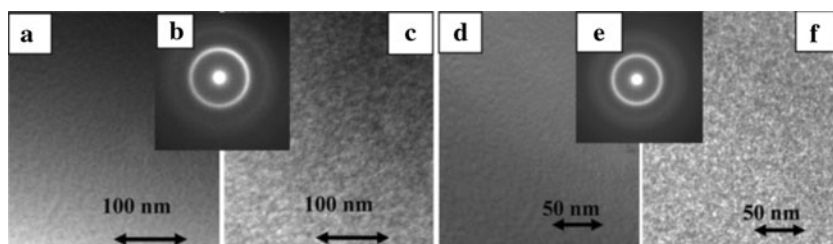

Fig. 4 Comparison of the DTA traces showing glass transition and complete crystallization process of the ribbons up to 1,100 K: **a** alloys Nb-1 and Nb-2; 5 and 10 at% Nb, 3% Al, **b** alloys Nb-2 and Nb-3; 10 at% Nb, increase of the Al content from 3 to 7 at., **c** alloys Nb-4 and Nb-5; increase of the Nb content to 20 and 25 at%, Al content 3 at%. The *arrows* mark annealing temperatures (see the text)
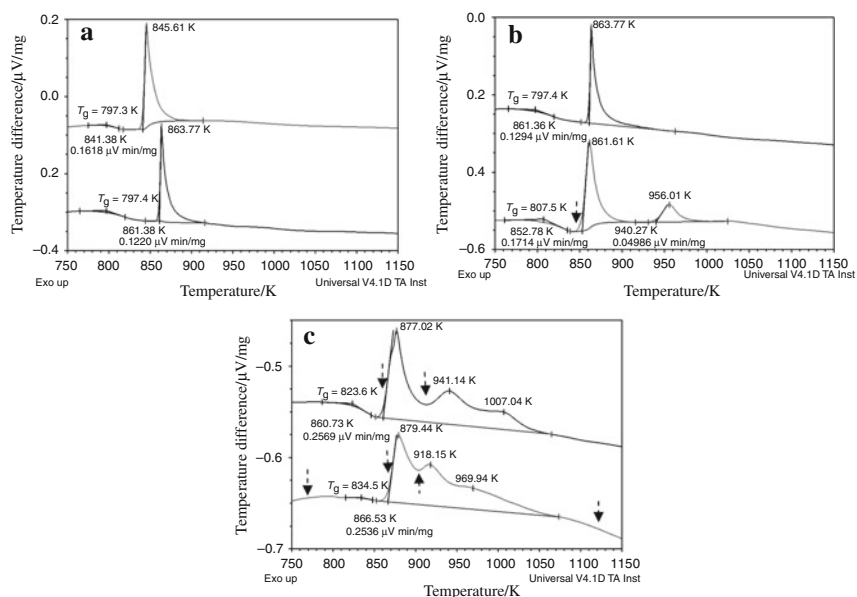
Table 2 Evolution of the glass transition and primary crystallization temperatures T_g and T_x, (rate 20 K/min), supercooled liquid range ΔT, reduced glass transition temperature T_g/T_m and reduced primary crystallization temperature $T_x/(T_g + T_l)$, (T_m—temperature of the melting, T_l—liquidus temperature)

	T_g/K	T_x/K	ΔT	T_g/T_m	$T_x/T_g + T_l$
Nb-1	797	841	44	0.62	0.40
Nb-2	797	861	64	0.61	0.41
Nb-3	807	853	46	0.62	0.40
Nb-4	824	861	37	0.62	0.40
Nb-5	835	867	32	0.63	0.39

Precision of the temperature determination better than ± 0.5 K

calorimeter. Also "in situ" heating in XRD equipment was applied.

The ribbon Nb-3 was annealed 120 s at 853 K (T_1 temp.), just at the start of the primary crystallization. The achieved XRD and microstructures are shown in the Fig. 5. As is shown the equiaxial crystalline grains of the average size of 55 nm formed in this case. Also ring-type of the respectful SADP confirmed that polycrystalline structure was formed. As resulted both from XRD and TEM, after applied annealing the amorphous phase completely disappeared, transforming to the crystalline. The phase which primary crystallized was identified as cubic (Pm-3m) NiTi(Nb), frequently noticed after crystallization of Ni-based amorphous alloys containing Ti, Zr, or Nb [4]. It's lattice constant a_0 was determined to be 0.299 nm.

The alloy Nb-4 was investigated after annealing and heated "in situ" at the temperature range of the primary crystallization with XRD. It was also studied by TEM after annealing in the calorimeter. Results are presented in Fig. 6. As is visible (Fig. 6a) some peaks connected to the first stages of crystallization were noticed only after short annealing at 922 K, that is at temperature between the first and the second peak (temp. T_2 in Fig. 4c). From the Fig. 6e–g results, that 360 s annealing at temperature 918 K, (near to T_2 temp., above T_p of the primary crystallization) was not enough for the complete crystallization, but long, 1,200 s annealing at temperature 865 K, near to T_x (T_1) temperature, caused complete crystallization of the amorphous phase.

The alloy Nb-5 was also studied after annealing at temperatures: 773 K (below T_g temperature), at $T_1 = 873$ short and long, and at 877 K, (near to the peak temperature), at $T_2 = 903$ K (between the first and the second crystallization effect) and at $T_3 = 1,123$ K, 50° above the end of the process of crystallization.

After 600 s annealing at temperature T_1 the Nb-5 amorphous phase revealed only small amount of nano-crystallization (Figs. 7c, 8a). As is seen crystallites up to 5 nm in diameter were formed at this temperature. Similar crystallites were observed also at temperature T_2. Even when crystallization was completed, due to the thermal curves at temperature T_3, not the complete transformation to the crystalline phase was observed but a large amount of the amorphous phase still remained (Figs. 7d, 8b–d).

The phases crystallizing in the range of the primary crystallization effects in alloys Nb-4 and Nb-5 are metastable in nature. Due to the XRD it was established that two phases crystallize first: cubic but distorted NiTi(Nb) and $Ni_{6.5}Nb_{6.5}$ of orthorhombic symmetry. At temperature above 922 K in the range of the second part of the thermal effect (Fig. 9c, d) the hexagonal phase $ZrNi_3$ crystallizes additionally.

The kinetics of the crystallization of the alloys Nb-2 and Nb-4

Two alloys, Nb-2 and Nb-4, differing only by the Nb increase on the account of Ti and Zr decrease (Table 1, Fig. 1) were chosen for the non-isothermal kinetics analysis. In Fig. 9 the DSC thermal curves for both alloys are compared on the scale of time and temperature. In the case of the Nb-2 ribbon the primary crystallization is completed after 20 s from the start of the effect and 14 s from the onset point, while in the case of Nb-4 alloy the observed process finishes after 106 s from the starting point and after 84 s from the onset point. It was assumed that the crystallization enthalpies for both alloys are proportional to the amount of the crystalline phase. The comparison of the enthalpies of transformation (Fig. 10) let to establish that in the case of the alloy Nb-4 only about 50% of crystalline phase may be achieved (Fig. 10c). Consequently 38 and 33% of crystallization was achieved at the peak temperature and heating

Fig. 5 a XRD results; **b**, **d** TEM microstructures and **c** SADP concerning the ribbon Nb- 3 after annealing 120 s at 853 K (T_1 temperature in Fig. 4): **b** BF, **d** DF. The phase NiTi(Nb) (cubic) was identified
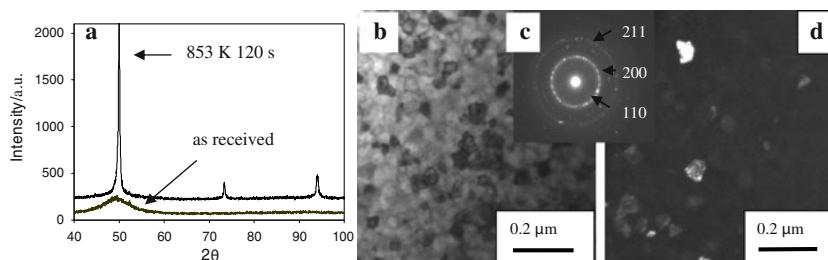
Fig. 6 XRD (**a**) and TEM
(**b**–**g**) showing crystallization of
the amorphous alloy Nb-4.
XRD-"in situ" heating and
annealing, TEM—samples
annealed in the calorimeter; **b**,
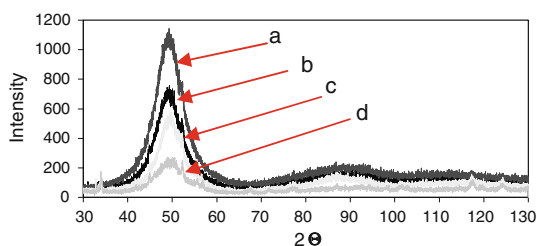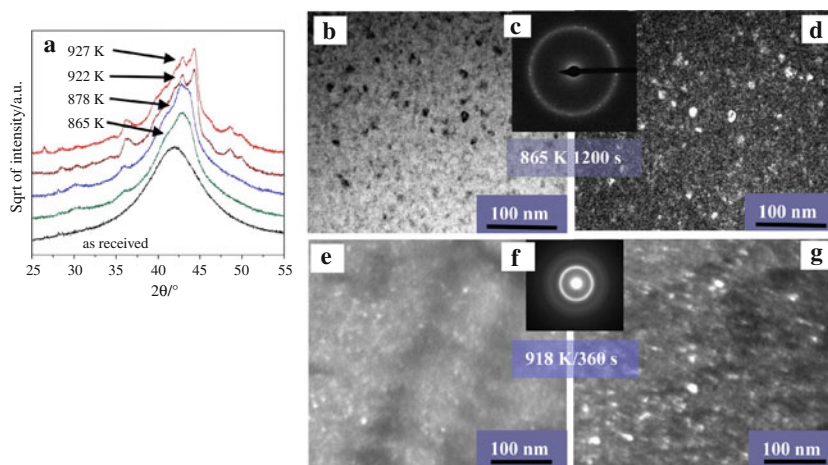**e** BF; **c**, **f** SADP; **c**, **g** DF

Fig. 7 XRD traces showing the crystallization of the amorphous
alloy Nb-5: (*a*) as received, (*b*) 300 s, 773 K, (*c*) 120 s, 873 K,
(*d*) 10 s, 1,123 K

rate 20 K/min for the alloys Nb-2 and Nb-4, respectively
(Fig. 9a, b).

The activation energy E for crystallization and growth
were determined for both alloys. The Kissinger [9] and
Ozawa [10] equations were used. As the fraction of
transformation at peak temperature T_p was changing for the
increasing heating rates, in case of the alloy Nb-2 the
activation energy was determined for peak temperature and
for the temperatures at which the constant amount of
transformation, 35 and 55% took place (Fig. 11). For the Nb-
2 alloy the activation energy was similar, 107.6 kcal/mol,
both for 35 and 55% of transformation and 110.0 kcal/mol
at T_p. The activation energy determined in a similar way from
Ozawa equation was slightly different; 111 kcal/mol for 35

and 55% of transformation and 113.7 kcal/mol for the peak
temperature (Table 3). The difference between respective
values were assumed to be the possible errors, of the E_A
values, that is ± 2 and ± 3 kcal/mol.

In case of the alloy Nb-4 two different peak tempera-
tures T_{p1} and T_{p2} were observed (Fig. 9c), related to the
nearly simultaneous crystallization of two different phases.
Like in previous alloy, at temperatures T_{p1} and T_{p2} the
fraction of the phase crystallized was not constant but
lowered with the heating rate increase (Table 3). Also,
because the determination of the T_{p1} temperature was less
certain with the increasing heating rate, two additional
temperatures at which 25 and 70% of transformation took
place, were chosen for the activation energy determination
(Fig. 12). As is presented in Table 3, the determined acti-
vation energy increased from 137 kcal/mol at 25% of
transformation, to 141 kcal/mol at T_{p1}, and 146 kcal/mol at
T_{p2}, further decreased to 140 kcal/mol at 70% of trans-
formation. Taking into account that at the temperature
range from the start of the crystallization until T_{p1} tem-
perature activation energy should concern predominantly
crystallization of the NiTi(Nb) phase (Fig. 10a), and at the
increasing temperatures till T_{p2}, the $Ni_{6.5}Nb_{6.5}$ phase
crystallization dominated, the variation of the apparent
activation may be explained. It should be expected that the
apparent activation energy changes from the value of
110 ± 2 kcal/mol for NiTi(Nb) phase to unknown value

Fig. 8 HREM and TEM
microstructures of the sample
Nb-5: **a** after annealing 600 s at
temperature $T_1 = 877$ K
(HREM); **b**–**d**) at temperature
$T_3 = 1,123$ K, **b** BF, **c** SADP,
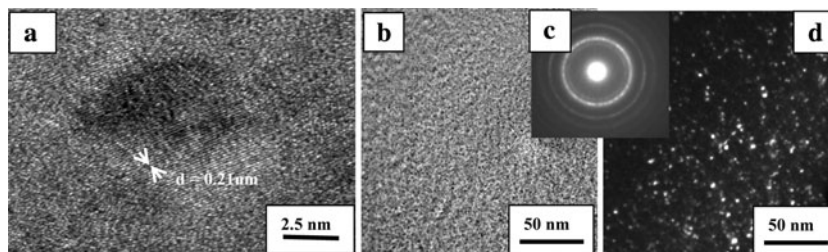**d** DF (TEM)

Fig. 9 Comparison of the DSC traces for the primary crystallization of the alloys Nb-2 (**a**, **b**) and Nb-4 (**c**, **d**) in the heat flow/temperature (**a**, **c**) and heat flow/time (**b**, **d**) axis. Rate 20 K/min
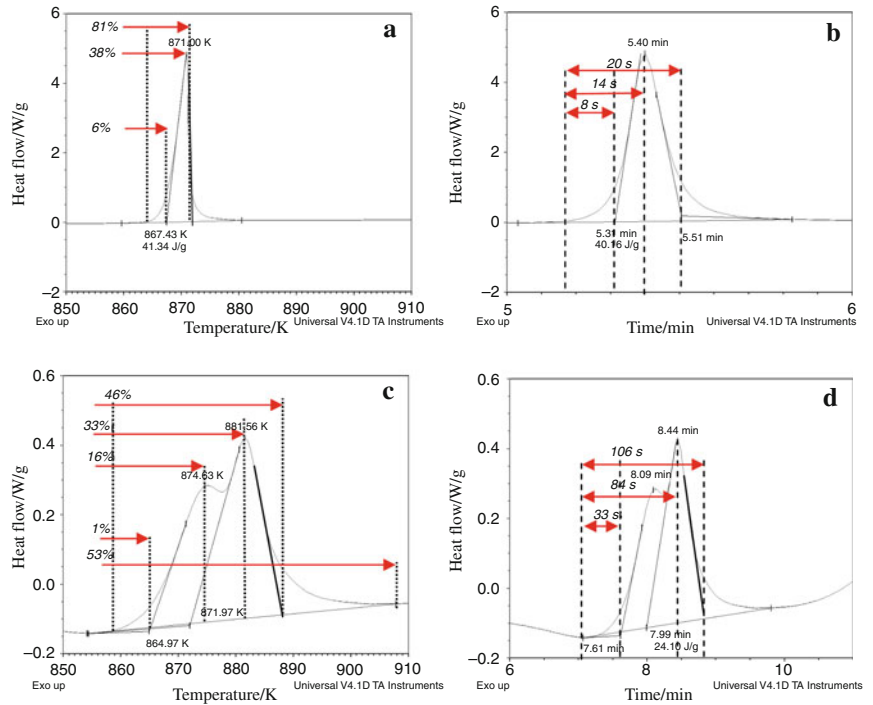

Fig. 10 The comparison of the enthalpies of crystallization of the Nb-2 and Nb-4 alloys (**a**, **b**) and determination of the average crystallization fraction versus the heating rate for the alloy Nb-4 (**c**)
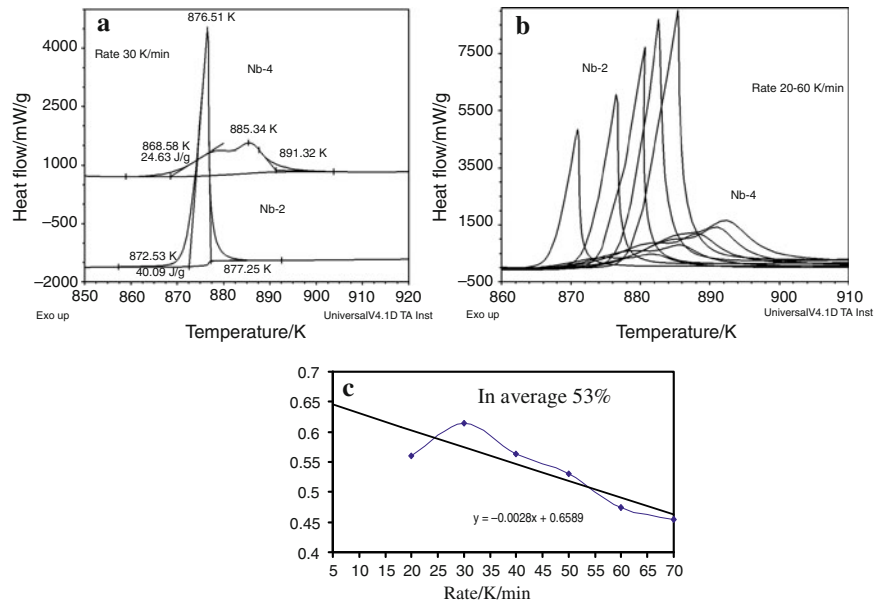

Fig. 11 The $\ln(\alpha/T^2)$ and $\ln(\alpha)$ vs. $1/T$ (α-heating rate) for the activation energy E_A determination with the **a** Kissinger, **b** Ozawa equations, for the alloy Nb-2
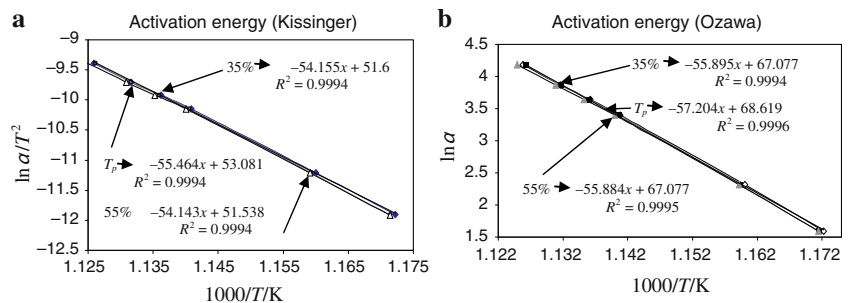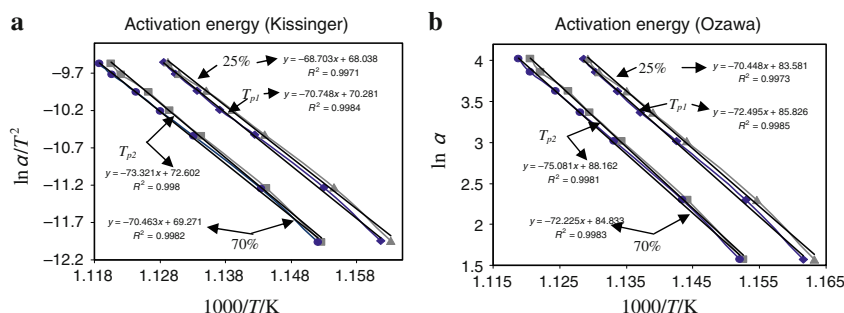
Table 3 Activation energy for crystallization and growth in alloys Nb-2 and Nb-4 determined with use of Kissinger [9] and Ozawa [10] equations

Alloy	Activation energy E_A/kcal/mol		
	Kissinger equation		Ozawa equation
Nb-2	35% of transformation	107.6	111.1
	At T_p (55–35% of transformation, heating rate dependent)	110.0 ± 2	113.7 ± 3
	55% of transformation	107.6	111.0
Nb-4	25% of transformation	136.5	140.0
	At T_{p1} (31–25% of transformation, heating rate dependent)	140.6 ± 4	144.1 ± 4
	At T_{p2} (67–60% of transformation, heating rate dependent)	145.7 ± 6	149.2 ± 6
	70% of transformation	140.0	143.5

Fig. 12 The $\ln(\alpha/T^2)$ and $\ln(\alpha)$ vs. $1/T$ (α-heating rate) for the activation energy E_A determination with the **a** Kissinger, **b** Ozawa equations, for the alloy Nb-4

for $Ni_{6.5}Nb_{6.5}$ phase, probably in the range of 146 ± 6 kcal/mol, both values multiplied by the volume fractions transformed to the particular structures. The values achieved with the Ozawa equation give the same tendency (Table 3).

Summary

1. Amorphous alloys of the composition $Ni_{58}Nb_x(ZrTi)_{1-x}$ Al_y, containing 5 to 25 at% Nb and 3 or 7 at% Al revealed increasing glass transition and primary crystallization temperature, decreasing supercooled liquid range, but stable GFA parameters.
2. Alloys containing more than 15 at% Nb undergo to complicated mechanism of crystallization. The mechanism characterizes by slow, not complete, multiphase crystallization, of the enthalpy about 50% smaller than in the remaining alloys from the series.
3. The first phases crystallizing in this alloys are NiTi(Nb) (cubic but distorted) and $Ni_{6.5}Nb_{6.5}$ (orthorhombic), as the last phase crystallizes Ni_3Zr (hexagonal).
4. The Kissinger and Ozawa equations give similar values of the activation energy for crystallization and growth of the NiTi(Nb) phase for the alloy Nb-2 with 10 at% Nb, 110 ± 2 and 113 ± 3 kcal/mol. The activation energy experimentally determined for the alloy Nb-4,

with 20 at% Nb concerns crystallization and growth of two different phases, NiTi(Nb) and $Ni_{6.5}Nb_{6.5}$. It reveals increasing tendency, from 141 ± 4 kcal/mol, at the range of temperatures where the predominant crystallization of the first phase proceeds, to 146 ± 6 kcal/mol, at temperatures in which the crystallization of the second phase dominates (values determined from the Kissinger equation).
5. Much higher thermal stability against crystallization of the alloys with high Nb content than in case of the alloys containing 5 and 10 at% Nb may be explained by the more complex diffusion process and larger apparent activation energy of the multi-phase crystallization, taking place while the amount of Nb exceeds 15 at%.

Conclusions

In case of the investigated Ni based, Nb containing alloys, crossing the 15 at% content of Nb leads to the distinct difference in primary crystallization process, concerning mechanism of crystallization as well as it's kinetics. The process is characterized by the parallel crystallization of two different phases and increasing value of the apparent activation energy for crystallization and growth. Such type of crystallization makes the alloys especially good for thermally stable bulk metallic glasses.

References

1. Inoue A, Shen B, Nishiyama N. Development and application of late transition metal bulk metallic glasses. In: Miller M, Liaw P, editors. Bulk metallic glasses. New York: Springer; 2008. p. 1–25.
2. Zhang W, Inoue A. Effects of Ti on the thermal stability and glass-formation ability of Ni–Nb glassy alloy. Mater Trans. 2002;43:2342–5.
3. Kimura H, Inoue A, Yamaura S, Sasamori K, Nishida M, Shinpo Y, Okouchi H. Thermal stability and mechanical strength of glassy and amorphous Ni–Nb–Zr alloys produced by rapid solidification. Mater Trans. 2003;44:1167–71.
4. Inoue A, Zhang W, Zhang T. Thermal stability and mechanical strength of bulk glassy Ni–Nb–Ti–Zr alloys. Mater Trans. 2002;43:1952–6.
5. Qiang JB, Zhang W, Inoue A. Quasicrystallization of $(Zr_{65}Al_{7.5}Cu_{27.5})_{95}Ti_5$ glassy alloy. Mater Trans. 2007;48:2385–9.
6. Zhang T, Inoue A. New bulk glassy Ni-based alloys with high strength of 3,000 MPa. Mater Trans. 2002;43:708–11.
7. Qiang JB, Zhang W, Inoue A. Ni–(Zr/Hf)–(Nb/Ta)–Al bulk metallic glasses with high thermal stabilities. Intermetallics. 2009;17:249–52.
8. Czeppe T, Ochin P, Sypień A, Major Ł. Crystallization and mechanical properties of the NiNb(ZrTi)Al amorphous alloys with10 and 25 at % of Nb and 3 to 7 at % Al content. J Phys Conf Ser. 2009;144(012038):1–4.
9. Kissinger HE. Reaction kinetics in differential thermal analysis. Anal Chem. 1957;29:1702–6.
10. Ozawa T. Kinetic analysis of derivative curves in thermal analysis. J Therm Anal. 1970;2:301.